Eur. Phys. J. A **12**, 317–325 (2001)

THE EUROPEAN PHYSICAL JOURNAL A

Complete and incomplete fusion in reactions of ^{7}Li + ^{56}Fe at E(^{7}Li) = 50 and 68 MeV from analysis of recoil range and light-particle measurements

R.I. Badran[1,a], D.J. Parker[2], and I.M. Naqib[3]

[1] Physics Department, The Hashemite University, P.O. Box 150459, Zarqa, Jordan
[2] School of Physics and Astronomy, University of Birmingham, Birmingham, B15 2TT, UK
[3] 12 Fogwell Road, Oxford OX2 9SA, UK

Received: 29 March 2001 / Revised version: 28 August 2001
Communicated by J. Äystö

Abstract. Excitation functions for the production of eight radioactive products of the reactions of ^{7}Li on ^{56}Fe have been measured up to $E(^{7}\mathrm{Li}) = 89$ MeV. Recoil range distributions for these products, together with inclusive proton, deuteron, triton and alpha spectra, have been measured at energies of 50 and 68 MeV. The α, t and d spectra show characteristic "break-up" components at forward angles, while the recoil distributions show evidence of complete fusion and incomplete-fusion process ^{56}Fe(^{7}Li,α)^{59}Co*. A parallel study on ^{55}Mn shows some evidences of the (^{7}Li,t) incomplete-fusion process, but the cross-section for this process is significantly less than for the triton fusion process. The recoil distributions can be reproduced on the assumption that essentially all the observed break-up fragments are in fact associated with incomplete fusion, but uncertainties in normalisation leave open the possibility of a significant contribution of pure break-up. A diffraction model of the (^{7}Li,α) transfer process reproduces the observed break-up α spectra with some success.

PACS. 25.70.-z Low and intermediate energy heavy-ion reactions – 25.70.Jj Fusion and fusion-fission reactions – 25.70.Hi Transfer reactions

1 Introduction

The mechanisms of heavy-ion nuclear reactions on medium-mass targets have been studied for many years. The dominant process is generally complete fusion, whereby the incident ion fuses with the target nucleus, forming an excited compound nucleus from which particles are subsequently evaporated. However, it has become increasingly apparent that in many cases there are significant contributions from incomplete-fusion processes, in which only part of the projectile fuses with the target nucleus to give an excited intermediate.

By measuring recoil range distributions of radioactive products as well as inclusive light-particle spectra, Parker *et al.* studied the contributions of complete and incomplete fusion to the formation of radioactive residues from the reactions of ^{12}C, ^{15}N, ^{16}O and ^{20}Ne on ^{51}V [1,2]. It was possible to predict accurately the residue data by assuming that essentially all of the non-evaporative components detected in the inclusive light-particle spectra were spectator fragments accompanying incomplete fusion, and modelling the subsequent evaporation.

[a] e-mail: rbadran_i@yahoo.com

The present work extends this approach to the entrance channel $^{7}\mathrm{Li} + ^{56}\mathrm{Fe}$, which shares the same complete-fusion compound nucleus as $^{12}\mathrm{C} + ^{51}\mathrm{V}$. It is well known that the loosely bound projectile ^{7}Li shows a tendency to break up (*e.g.*, into $\alpha + \mathrm{t}$) in proximity to the target and it is interesting to examine how this affects the occurrence of incomplete fusion.

As a background to this work, the excitation functions for the production of eight radioactive products were first measured over the energy range up to 89 MeV. Two energies, 50 and 68 MeV were then selected for detailed study, and recoil range distributions and light-particle spectra were measured at these energies. The measurement and analysis techniques were generally similar to those described previously [1,2] and are briefly summarised here.

2 Experimental method

2.1 Excitation functions

The excitation functions for the production of the eight radioactive products ^{61,60}Cu, ^{60,58,57,56}Co and ^{54,52}Mn were

measured by irradiating a stack of natural-iron foils with an 89 MeV $^{7}Li^{3+}$beam from the Harwell VEC, followed by off-line γ-ray spectrometry. The stack comprised 24 foils each of nominal thickness 12.5 μm, the actual thickness of each foil being determined by weighing. The stack of foils was mounted inside an electrically-suppressed Faraday cup and irradiated at a current of approximately 5 particle nA to a total fluence of 80 particle μC, with a record of fluence *vs.* time being kept.

At the end of irradiation process the foils were counted in turn for 100 s at a distance of 200 mm from a 13.5% efficient Ge (Li) detector, whose photopeak efficiency had previously been measured as a function of energy. After 6 hours, the foils were counted again but at a distance of 75 mm. On the following day, a 300 s count was performed, and a week later a 3000 s count was performed. Finally, after 2 months, a long count (at least 50000 s) was performed on each foil in order to determine the ^{60}Co activity.

The activity of each product detected was obtained from the measured count rates using the known detector efficiency and published γ-ray branching ratios [3]. For products emitting more than one strong γ-ray line, a weighted average was used. The published half-life was used to extrapolate the activity back to the end of irradiation, and then this activity was converted to a cross-section using the foil thickness and the total beam fluence. For short-lived products, which decayed significantly during irradiation, a correction was applied based on a saturation factor determined from the variation in fluence with time during irradiation. The uncertainty in the final cross-section is dominated by the uncertainty in determining the foil thicknesses and is estimated at 10%. Finally, the beam energy on exit from each foil was determined from the foil thicknesses and a parameterization of the range/energy curve of Littmark and Ziegler [4] for ^{7}Li in iron.

2.2 Light-particle spectra

The inclusive energy spectra of protons, deuterons, tritons and alphas emitted in reactions of a ^{7}Li beam, with a natural-iron target, were measured at incident energies of 50 and 68 MeV and at laboratory angles ranging from 10° to 150°. The target used had a nominal thickness of 2.5 μm and was mounted normal to the beam except during the measurement of spectra close to 90° when the target angle was displaced by 15°. The transmitted beam was collected in an electrically-suppressed Faraday cup mounted downstream from the target.

Particle identification was achieved using a $\Delta E - E$ telescope of two silicon detectors: a 15 μm ΔE detector was used for most of the measurements, but a 100 μm ΔE detector was used to measure the deuteron spectra at forward angles and the proton spectra above 8 MeV, a 3000 μm E detector being used throughout. The signals from the detectors were digitized and recorded event-by-event on a computer. Subsequently, they were sorted into maps of total energy $E + \Delta E$ *vs.* a characteristic particle identifier. In this way, the various light particles could be easily distinguished and the total energy spectrum for each type of particle was extracted.

Energy calibration was performed using the elastically scattered ^{7}Li detected at forward angles, with appropriate correction for energy loss in the target. The absolute normalisation of the spectra may be systematically uncertain by up to 15%. This is due principally to uncertainties in the detector solid angle and the target thickness.

2.3 Projected recoil range distributions

The recoil range distributions, projected parallel to the beam axis, for the principal radioactive products were measured at incident energies of 50 and 68 MeV by irradiating a thin iron target backed by a stack of thin aluminium catcher foils. For each irradiation, the target consisted of approximately 50 μg/cm^2 Fe evaporated onto a support of 100 μg/cm^2 aluminium. The target was mounted with the iron layer downstream and followed immediately by a stack of 25 evaporated aluminium catcher foils, each having thickness between 40 and 100 μg/cm^2. The thickness of each catcher foil was determined prior to its use, to an uncertainty of approximately 5%, by measuring the energy lost by 5.8 MeV alpha-particles from a ^{244}Cm source in traversing the foil. The total fluence was approximately 1000 particle μC.

Following each irradiation, the catcher foils were counted in turn against the face of a 25% efficient Ge (Li) detector at intervals over a period of several weeks. Only the strongest γ-ray line was used to quantify each product. The distribution through the catcher stack was obtained by dividing the count rate measured in each catcher, corrected for elapsed time, by the thickness of each catcher. These measurements were thus purely relative. The absolute normalization for each recoil distribution is taken from the cross-section determined during the previous excitation function measurement.

3 Results and analysis

3.1 Excitation functions

Figure 1 shows the measured excitation functions for the formation of eight radioisotopes (^{61,60}Cu, ^{60,58,57,56}Co, ^{54,52}Mn). The smooth solid curves represent the predictions of the statistical model code CASCADE [5]. In this calculation, complete fusion is assumed for ^{7}Li projectiles within the bounds of the hard grazing partial wave $\ell_{\rm g}$, which was derived from the liquid-drop potential formulation of Wilczynski and Siwek-Wilczynska [6,7]. As in the previous work [2], the CASCADE calculations were performed using the parameters (set F) recommended by Kicinska-Habior *et al.* [8] following their study of the ^{63}Cu compound nucleus, and with the extended form of the code which includes the giant dipole and both the isoscalar and the isovector giant quadrupole resonances.

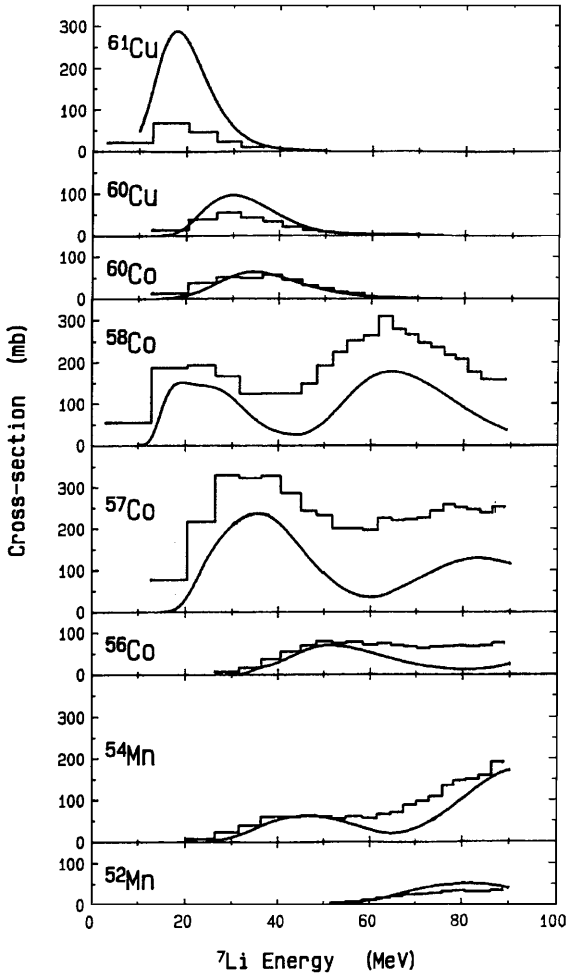

Fig. 1. Excitation functions for the production of eight radioisotope products of the reactions of ^{7}Li on ^{56}Fe (histograms). The curves show the results of the CASCADE statistical model calculations.

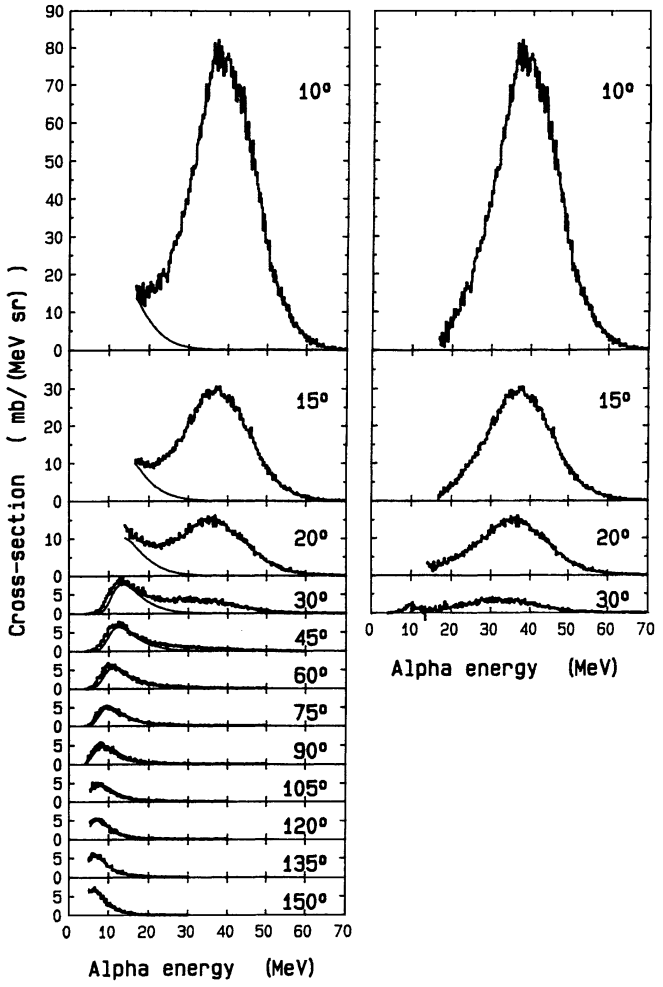

Fig. 2. Left-hand panel: The α-particle spectra measured at 12 laboratory angles from the reaction of 68 MeV ^{7}Li on ^{56}Fe. The curves show the evaporative component, as modelled by CASCADE and fitted to the backward-angle data. Right-hand panel: The break-up α-particle spectra obtained by subtracting the curves in left-hand panel from the data.

Figure 1 shows that the general shapes of the excitation functions and the locations of their peaks are fairly well reproduced by the CASCADE calculation. In effect, each peak location corresponds to the excitation energy of the ^{63}Cu* nucleus related to the separation energy of the particles that need to be evaporated to produce the residue in question. For example, the energy of the first peak in the ^{58}Co excitation function corresponds to the separation of an alpha and a neutron; while the second peak corresponds to the separation of three neutrons and two protons.

In general the calculation also predicts quite well the magnitude of the cross-sections for forming the residues. However, it significantly overestimates the cross-section for the formation of ^{61}Cu and to a lesser extent that for ^{60}Cu. The cross-sections for ^{58}Co and ^{57}Co are, on the other hand, underestimated. The significant discrepancy between measured and calculated cross-sections for the formation of ^{61}Cu is probably due to the strong dependence of this product on the relatively small, but not accurately estimated, probability of gamma decay at high excitation energies. The discrepancies between the measured and calculated excitation functions for ^{58}Co and ^{57}Co can be attributed to additional contributions from incomplete-fusion processes such as ^{56}Fe(^{7}Li,α)^{59}Co*, which are discussed below.

3.2 Light-particle energy spectra

The alpha spectra measured at 50 MeV were presented in ref. [12]. Figure 2 shows the corresponding spectra at 68 MeV, the deuteron and triton spectra are shown in figs. 3-4, and the proton spectra measured at 50 MeV in fig. 5.

The forward-angle deuteron, triton and alpha spectra all show a pronounced "break-up" component, centred approximately at beam velocity, whose intensity falls off rapidly with angle. The proton, deuteron and alpha spectra include a characteristic evaporative component,

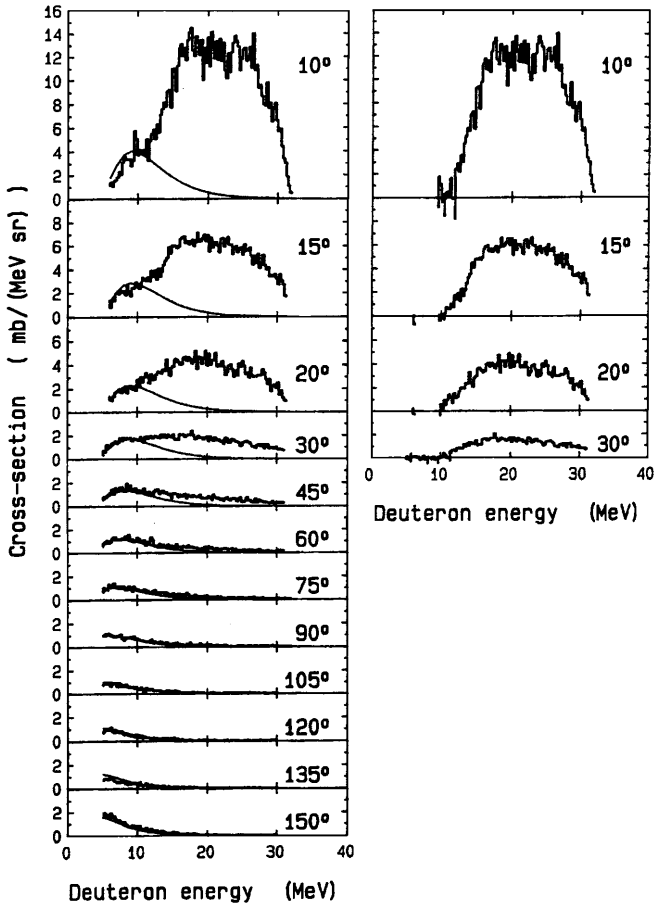

Fig. 3. As fig. 2, for the deuteron spectra measured at 68 MeV.

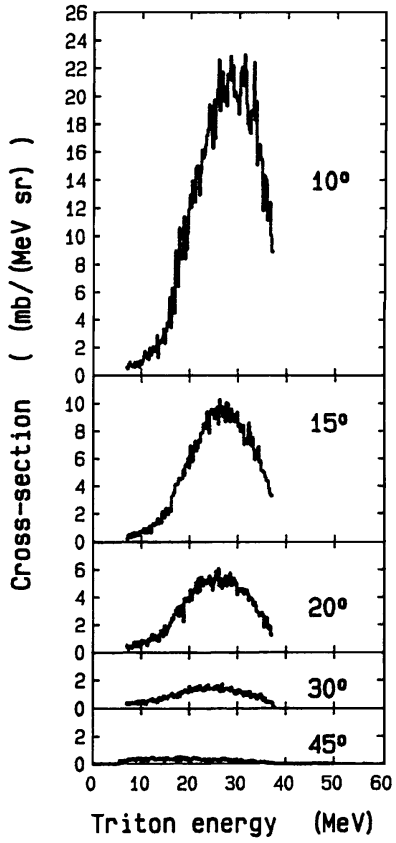

Fig. 4. The triton spectra measured at forward angles from the reaction of 68 MeV ^{7}Li on ^{56}Fe.

to which the spectra predicted by CASCADE have been fitted. CASCADE gives the energy spectra of evaporated particles but not their angular distribution, which must, however, be symmetric about 90° in the centre-of-mass frame. This centre-of-mass angular distribution was therefore assumed to be of the form $a\{1 + c/\sin\phi\}$, and the parameters a and c were determined by transforming into the laboratory frame and fitting to the spectra measured at backward angles. Good fits at backward angles were obtained in this way. At forward angles, subtracting the fitted evaporative component from the alpha and deuteron spectra leaves just the break-up components shown in figs. 2 and 3 (right-hand panels).

An anomaly is apparent in the forward-angle proton spectra, which contain a long high-energy tail superimposed on the fitted evaporative component. This does not appear to be close to beam velocity, and cannot be accounted for on the basis of evaporation from either the compound nucleus or an incomplete-fusion intermediate (the lower recoil velocity of the latter will result in a less pronounced forward/backward asymmetry in the laboratory frame than evaporation following complete fusion). It would appear to be due to emission from a source moving faster than the recoiling compound nucleus, and may correspond to some sort of pre-equilibrium process.

Table 1 shows the total yields of evaporated particles and break-up fragments deduced from the measured spectra (all considered accurate to ±15%). It can be seen that significantly fewer evaporated alphas than expected were detected; this anomaly will be discussed later. In each case, the yield of break-up fragments was found to fall off exponentially with angle as $\exp(-\frac{\theta}{\theta_0})$ (the values of θ_0 being listed in table 1) so that the total yield could be determined by extrapolation to 0°. The most striking result is that significantly more break-up alphas were detected than deuterons and tritons combined, which implies that these are not simply fragments from pure projectile break-up but that, in many cases, when an alpha is emitted the remainder of the projectile fuses with the target. This ^{7}Li(^{56}Fe,α)^{59}Co* incomplete-fusion process is apparently significantly more important than the corresponding process in which a triton (or possibly a deuteron) is emitted. However, from the inclusive particle spectra alone one cannot draw any conclusions as to whether the detected deuteron and triton fragments arise from pure break-up or incomplete fusion.

3.3 Differential range distributions

The solid histograms in figs. 6 and 7 show the recoil range distributions measured for a number of radioactive residues at 50 MeV and 68 MeV beam energy. The

Table 1. Yields of evaporative and break-up particles in the measured spectra.

	Alphas		Tritons		Deuterons		Protons	
Incident energy (MeV)	50	68	50	68	50	68	50	68
Measured evaporative yield (mb)	490	670			55	140	930	1560
Ratio of measured/predicted evaporative yield	0.59	0.64					0.74	1.03
Angle constant θ_0 for breakup component (degrees)	10.1	6.8	11.8	7.8	14.1	10.4		
Measured break-up yield (mb)	490	550	110	150	90	95		

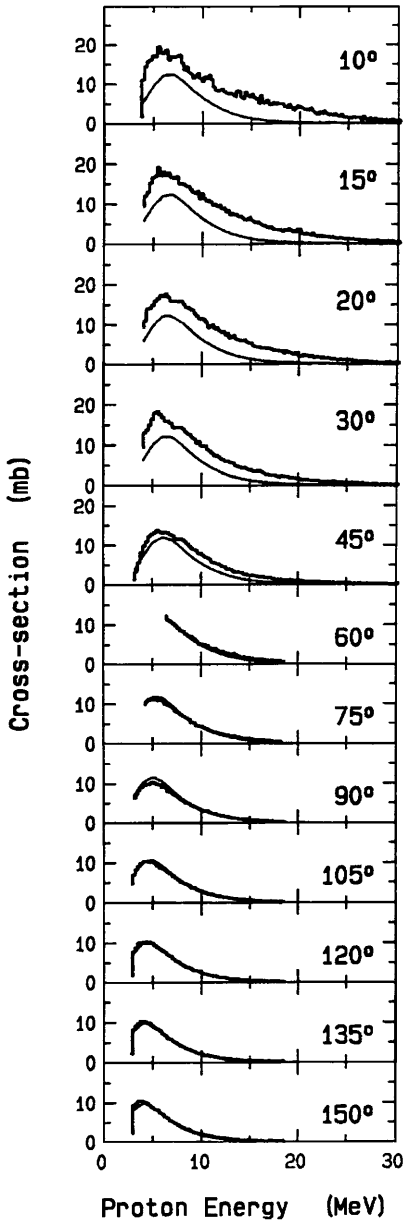

Fig. 5. The proton spectra measured at 12 laboratory angles from the reaction of 50 MeV ^{7}Li on ^{56}Fe. The curves show the evaporative component, as modelled by CASCADE and fitted to the backward-angle data.

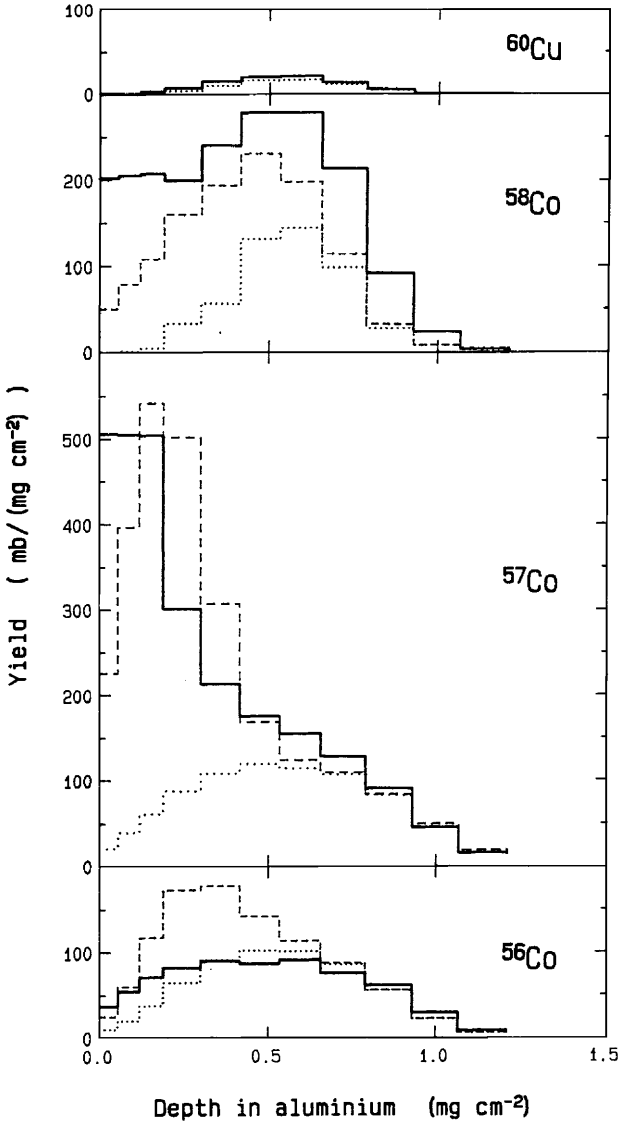

Fig. 6. The recoil range distributions measured for four products from the reaction of 50 MeV ^{7}Li on ^{56}Fe (solid histograms). The dotted histograms show the corresponding distributions modelled assuming complete fusion. The dashed histograms show the distributions modelled on the assumption that all of the observed break-up fragments are associated with incomplete fusion.

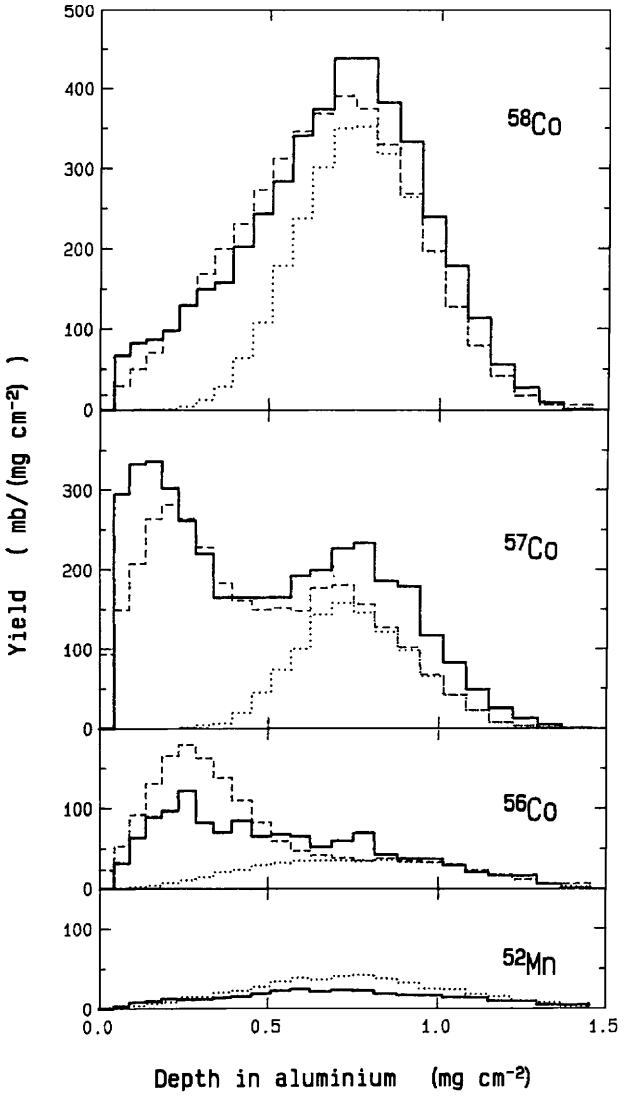

Fig. 7. As fig. 6, for four products from the reaction of 68 MeV ^{7}Li on ^{56}Fe.

dotted histograms show the predicted contribution from complete fusion: as in previous work [2], a Monte Carlo approach was used to model the recoil distribution expected following evaporation of a specified sequence of particles from the recoiling compound nucleus. Here, the resulting distributions have been normalised to the cross-sections predicted by CASCADE. The complete-fusion contributions, which are all centred on the same depth, agree well with the measured distributions in the case of ^{60}Cu (at 50 MeV) and ^{52}Mn (at 68 MeV). In the case of the other residues, complete fusion satisfactorily accounts for the deeper parts of the recoil distributions but there are clearly additional shallower components, which may be attributed to incomplete fusion in which less recoil momentum is transferred to the intermediate.

To model the incomplete-fusion contributions to the recoil distributions, we start by making the extreme assumption that essentially all of the "break-up" observed in the light-particle spectra is in fact incomplete fusion, so that, whenever a projectile fragment (α, d or t) is detected, it is assumed that the remainder of the projectile fused with the target. As in previous work, for the purposes of modelling the recoil distributions, the observed break-up spectra have been approximated by the empirical form

$$\frac{\mathrm{d}^2\sigma}{\mathrm{d}E\mathrm{d}\Omega} = \sigma_0 \exp\left[-\frac{\theta}{\theta_0}\right]\left(\exp\left[\frac{E-(E_0-k_1\theta-k_2\theta^2)}{\omega_1}\right] + \exp\left[\frac{E+(E_0-k_1\theta-k_2\theta^2)}{\omega_2}\right]\right),$$

where the parameters θ_0, E_0, k_1, k_2, ω_1, ω_2 and σ_0 were obtained by least squares fitting to the data. A Monte Carlo approach was then used to simulate the initial distribution of excitation energies, velocities and angles for the corresponding incomplete-fusion intermediate. This approach was also used to model the recoil distribution after subsequent evaporation. Here, the distribution of excitation energies was combined with CASCADE calculations in order to predict the yields of individual residues. This was done using the approximation that incomplete fusion imparts angular momentum $2m\bar{h}$ to the excited intermediate, where m is the mass of the fused fragment in atomic-mass units. The summed contributions to the production of each residue from the various incomplete-fusion reactions were then added to the relevant complete-fusion contribution, and the results are shown as dashed histograms in figs. 6 and 7. The agreement with the data is very satisfactory, bearing in mind that no fitting is involved: these are absolute predictions of the recoil distributions on the assumption that all of the observed break-up fragments correspond to incomplete fusion.

The agreement vindicates the hypothesis that the majority of the observed break-up α-particles are due to the incomplete-fusion process ^{56}Fe(^{7}Li,α)^{59}Co*. However, the evidence for the process ^{56}Fe(^{7}Li,t)^{60}Ni* is less clear cut, since this intermediate will in any case not strongly populate the particular radioactive residues observed. In order to obtain more direct evidence for the occurrence of this process in a very similar system, a separate measurement of recoil range distributions was made using a ^{55}Mn target: in fig. 8 the results (solid histograms) are compared to the shapes of the distributions expected following evaporation from the complete-fusion compound nucleus ^{62}Ni* (dashed histograms). There is an uncertainty of around 25% in the normalisation of the experimental distributions, and for clarity the modelled distributions have been normalised so as to fit the data. The interesting feature of these distributions is the small additional component at low-momentum transfer in the ^{57}Co distribution, which cannot be due to triton fusion (populating the intermediate ^{58}Fe*) and must be attributed to the incomplete-fusion process ^{55}Mn(^{7}Li,t)^{59}Co*. We conclude that the alpha fusion process does indeed occur in these systems, but that the total cross-section for this process is very much smaller (by around a factor 5) than for the triton fusion process.

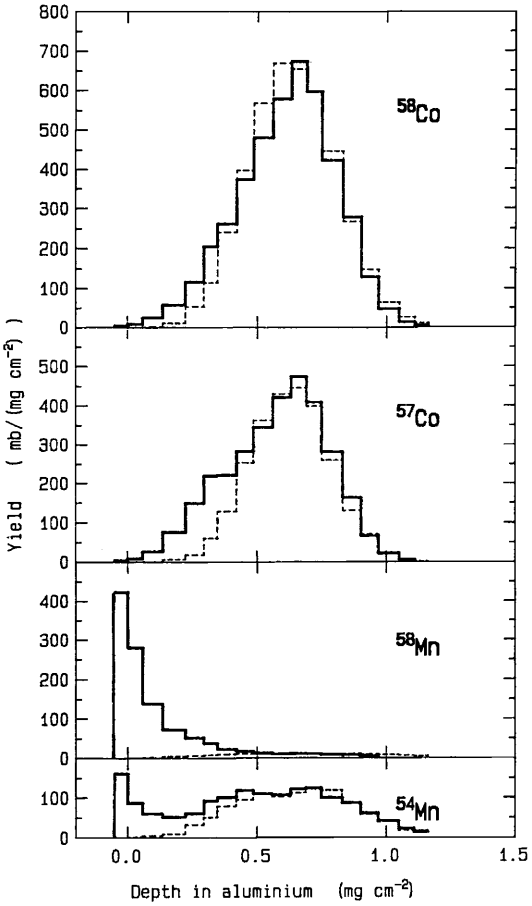

Fig. 8. The recoil distributions measured for four products from the reaction of 50 MeV ^{7}Li on ^{55}Mn. The dashed histograms show the modelled contribution from complete fusion (normalised to the data).

3.4 Analysis of break-up alpha spectra

On the basis that most of the break-up component in the alpha-particle spectra corresponds to incomplete fusion, we have attempted to calculate the form of these spectra using single-step transfer reaction theory. The approach, which is based on the DWBA approach, modified as suggested by Mermaz [9–11] to allow transfer to continuum states using a diffraction approximation, was described in a previous paper [12] where we presented the results at 50 MeV. Here we summarise the main features and extend the work to 68 MeV.

The double differential cross-section in the centre-of-mass frame for a quasi-elastic transfer reaction (involving zero-spin nuclei, an angular-momentum transfer $\boldsymbol{J}$ and leaving the residual nucleus at an excitation energy E^*) to the continuum states, was written in the form [9–12]

$$\frac{\mathrm{d}^2\sigma}{\mathrm{d}\Omega \mathrm{d}E_\mathrm{f}} = \sum_J \rho(0,E^*)(2J+1) \times \exp\left[-\frac{J(J+1)}{2\sigma^2}\right]\sigma(\theta,E_\mathrm{f},J)\,, \quad (1)$$

where $\rho(0,E^*)$ is the density of zero-spin levels at excitation energy E^* in the residual nucleus and σ^2 is the spin cut-off parameter. $\sigma(\theta,E_\mathrm{f},J)$, the cross-section of the transfer reaction leading to a final state of definite spin J and excitation energy E, is taken to be the single-step finite no recoil Distorted Wave Born (DWBA) cross-section [9,12]:

$$\sigma(\theta,E_\mathrm{f},J=L) = \frac{\mu_\mathrm{f}\mu_\mathrm{i}}{(2\pi\hbar^2)^2}\frac{k_\mathrm{f}}{k_\mathrm{i}}\sum_M \left|T_L^M\right|^2\,, \quad (2)$$

where

$$T_L^M = \tau\frac{4\pi}{k_\mathrm{i}k_\mathrm{f}}\sum_{\ell_\mathrm{i}\ell_\mathrm{f}} i^{\ell_\mathrm{i}-\ell_\mathrm{f}-L}\beta_{\ell_\mathrm{i}\ell_\mathrm{f}}(2\ell_\mathrm{f}+1)^{\frac{1}{2}} \times \exp\left[i(\sigma_{\ell_\mathrm{i}}+\sigma_{\ell_\mathrm{f}})\right] \times\langle \ell_\mathrm{f}L;00|\ell_\mathrm{i}0\rangle\langle\ell_\mathrm{f}L;-MM|\ell_\mathrm{i}\rangle Y_{\ell_\mathrm{f}}^{-M}(\theta,0)\,. \quad (3)$$

Here ℓ is the partial wave, μ is the reduced mass, k is the wave number, σ_ℓ is the Coulomb phase shift, and τ is a spectroscopic transfer parameter. The subscripts i and f refer to the entrances and exit channels, respectively. The form of the reduced matrix element $\beta_{\ell_\mathrm{i}\ell_\mathrm{f}}$ was developed by Austern and Blair for inelastic scattering of strongly absorbed projectiles and modified by Hahne [13] for transfer reactions, namely

$$\beta_{\ell_\mathrm{i}\ell_\mathrm{f}}(k_\mathrm{i},k_\mathrm{f}) = \frac{1}{2i}(E_\mathrm{i}E_\mathrm{f})^{\frac{1}{2}}\left[\frac{\partial S(\ell_\mathrm{i}-\ell_{\mathrm{g_i}})}{\partial\ell_\mathrm{i}}\frac{\partial S(\ell_\mathrm{f}-\ell_{\mathrm{g_f}})}{\partial\ell_\mathrm{f}}\right]^{\frac{1}{2}}. \quad (4)$$

Here ℓ_g is the grazing angular momentum, and S_ℓ is the scattering matrix element which is expressed as $\eta_\ell e^{2i\delta_{\ell,\mathrm{N}}}$ (where η_ℓ is the reflection coefficient and $\delta_{\ell,\mathrm{N}}$ is the nuclear phase shift of the ℓ-th partial wave). Neglecting terms in $\frac{\partial S_{\ell,\mathrm{N}}}{\partial\ell}$, this expression [12] takes the form

$$\beta_{\ell_\mathrm{i}\ell_\mathrm{f}}(k_\mathrm{i},k_\mathrm{f}) = \frac{1}{2i}(E_\mathrm{i}E_\mathrm{f})^{\frac{1}{2}} \times\exp\left[2i(\delta_{\ell_\mathrm{i},\mathrm{N}}+\delta_{\ell_\mathrm{f},\mathrm{N}})\right]\left[\frac{\partial\eta_{\ell_\mathrm{i}}}{\partial\ell_\mathrm{i}}\frac{\partial\eta_{\ell_\mathrm{f}}}{\partial\ell_\mathrm{f}}\right]^{\frac{1}{2}}. \quad (5)$$

Expression (5) differs from that used by Mermaz in that the exponential factor involving the nuclear phase shifts appears explicitly. Combination of (5) and (3) yields an expression for the transition amplitude similar to that used by Mermaz except that the factor $\exp(\sigma_{\ell_\mathrm{i}}+\sigma_{\ell_\mathrm{f}})$ becomes $\exp(\delta_{\ell_\mathrm{i}}+\delta_{\ell_\mathrm{f}})$, where $\delta_\ell=\sigma_\ell+\delta_{\ell,\mathrm{N}}$ [12]. However, the nuclear phase shifts $\delta_{\ell,\mathrm{N}}$ were introduced separately in the calculations by Mermaz as a means of accounting for the refractive effects of the nuclear potential and improving the fit to the data.

The McIntyre parameterisation [14] was used for the reflection coefficients and the nuclear phase shifts $\delta_{\ell,\mathrm{N}}$ in the entrance channel as

$$\eta_\ell = \left(1+\exp\frac{(\ell_\mathrm{g}-\ell)}{\Delta}\right)^{-1}, \quad (6)$$

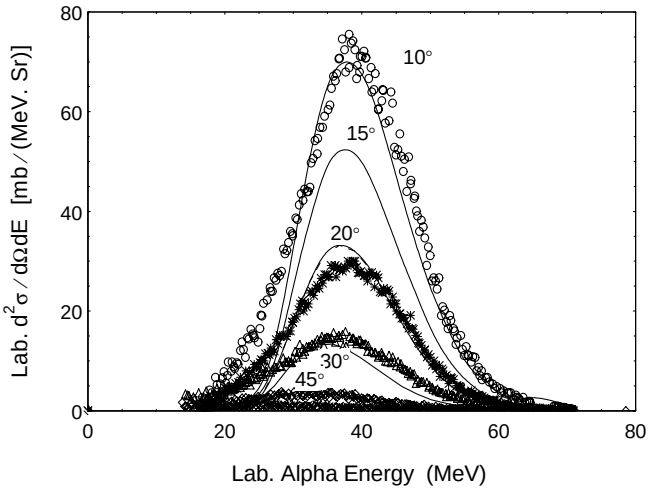

Fig. 9. The direct components of alpha-particle spectra from the reaction of 68 MeV ^{7}Li on ^{56}Fe measured (○, ∗, △, × and +) at 10°, 15°, 20°, 30° and 45° laboratory angles, respectively, are compared to the calculated (corresponding solid curves) double differential spectra.

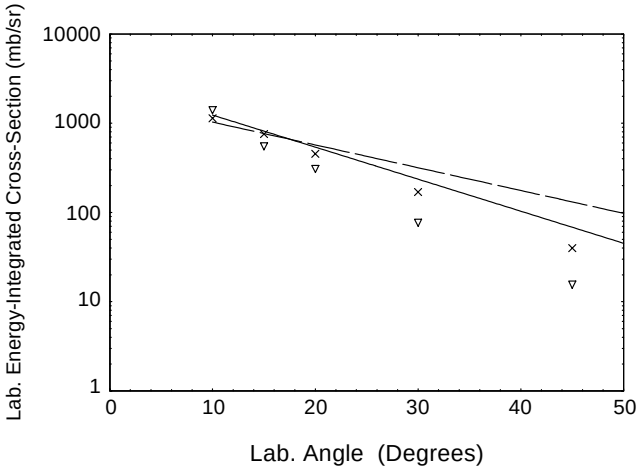

Fig. 10. Comparison of experimental (× and ▽ symbols) and calculated (dashed and solid curves) laboratory angular distribution of energy-integrated cross-section of the transfer reaction ^{56}Fe(^{7}Li,α)^{59}Co at 50 and 68 MeV, respectively.

$$\delta_{\ell,\mathrm{N}} = \mu \left(1 + \exp \frac{(\ell - \ell'_{\mathrm{g}})}{\Delta'}\right)^{-1}, \qquad (7)$$

with similar relations for the exit channel. Here Δ (or Δ') measures the nuclear surface diffusivity and ℓ_{g} (or ℓ'_{g}) is the grazing angular momentum in ℓ-space and μ is a measure of the refractive strength of the nuclear potential. The relations between ℓ_{g} and the nuclear radius R and between Δ and the diffusivity in radial space d were derived by Frahn [15]:

$$\ell_{\mathrm{g}} = kR \left[1 - \frac{2n}{kR}\right]^{\frac{1}{2}}, \qquad (8)$$

$$\Delta = kd \left(1 - \frac{n}{kR}\right) \left(1 - \frac{2n}{kR}\right)^{\frac{1}{2}}. \qquad (9)$$

Here $n = \frac{Z_1 Z_2 e^2}{\hbar \nu}$ is the Sommerfeld parameter; $R = r_0(A_1^{\frac{1}{3}} + A_2^{\frac{1}{3}})$, where A_1 and A_2 are mass numbers and Z_1 and Z_2 the atomic numbers of the pair of nuclei in the entrance or exit channels of the reaction.

The same values used previously (parameter set 1 of ref. [12]) for the three McIntyre parameters r_0, d and μ in the entrance and exit channels were adopted. These were obtained by fitting the calculated angular distribution for elastic scattering of ^{7}Li on ^{54}Fe (48 MeV) and ^{4}He on ^{58}Ni (43 MeV) to the available published data ([12] and references therein). The only free parameter in the calculations is then the level density parameter a: at $E(^{7}\mathrm{Li}) = 50$ MeV the value $a = \frac{A}{13} = 4.54$ MeV^{-1} was adopted but at 68 MeV better agreement with the data is found using the slightly smaller value $a = \frac{A}{15}$ MeV^{-1}. In fig. 9 the calculated spectra are compared to the direct component of the measured spectra; the normalisation constant τ has been chosen to match the data at 10° and corresponds to a total cross-section for this transfer process of 0.54 barn.

It is clear that although the calculation satisfactorily predicts the shape of the energy spectrum at each angle, the measured spectra fall off with angle much faster than the calculations predict. This effect is shown in fig. 10, where the energy-integrated cross-sections are plotted against laboratory angle; the results previously reported at 50 MeV are also plotted in this figure. In both cases the calculations significantly underestimate the rate of the exponential fall-off with angle, although they do correctly predict that this fall off is faster at 68 MeV than at 50 MeV. As reported previously [12], the discrepancy can be reduced by increasing the nuclear phase factor parameters μ significantly from the values deduced from the elastic-scattering data. It is not surprising that a model based essentially on a perturbative development from elastic-scattering data should underestimate the effect of the nuclear field in deflecting the trajectories involved in incomplete fusion towards forward angles.

4 Conclusions

The observed inclusive α, t and d spectra show major contributions at forward angles of the form expected from the break-up of the projectile. Significantly more alphas are present than deuterons + tritons combined, indicating that a major part of the alpha yield corresponds to incomplete fusion rather than pure break-up. The recoil range distributions of several of the radioactive products show a distinctive contribution from the ^{56}Fe(^{7}Li,α)^{59}Co* incomplete-fusion process. Diffraction model calculations of this process reproduce the non-evaporative component of the experimental spectra well, except that the experimental spectra fall off more rapidly with angle.

Making the extreme assumption that whenever a projectile fragment is detected its partner must have fused

with the target, and modelling the subsequent evaporation stage using previously adopted parameters in the statistical model code CASCADE, reproduces the yields and recoil distributions of all the radioactive residues detected at 50 and 68 MeV very well. However, the particular residues studied are not very sensitive to the contribution of the ^{56}Fe(^{7}Li,t)^{60}Ni* process. The recoil distributions measured at 50 MeV on a ^{55}Mn target confirm the presence of this process, but indicate a cross-section around a factor of 2 lower than the total d + t break-up yield. Thus, while establishing that the majority of "direct" alphas are associated with incomplete fusion of the triton, our data allow the possibility that there is around 100 mb of pure break-up.

Anomalous yields of protons are observed at the most forward angles, which may be attributable to pre-equilibrium processes. The measured yields of evaporated particles (particularly alphas) are in general significantly lower than predicted by the CASCADE calculations, even though the latter satisfactorily reproduce the observed residue yields. When modelling these spectra, adding the relatively small contribution of particles evaporated following incomplete fusion would slightly increase this discrepancy.

There are three possible explanations for this inconsistency, none of which alone is entirely satisfactory:

1) The total cross-section for complete fusion may be smaller than assumed, due to competition from incomplete fusion (or pure break-up) inside the hard grazing limit. There is no indication of a serious overestimate in the complete-fusion contribution to the recoil distributions, but it is possible that the normalisation of these distributions (which comes from the excitation function measurement) may be somewhat high.
2) The CASCADE calculations may exaggerate the importance of alpha evaporation. Again, the recoil distributions provide no evidence of this, and it should also be noted that using the same parameters CASCADE correctly predicted the evaporative alpha yields from reactions of four different projectiles on ^{51}V at 6 MeV/u [2]. Alpha evaporation is particularly important from high angular momentum states, so that reducing the total fusion cross-section as in (1) will reduce the yield of alphas more than protons.
3) The normalisation of the measured particle spectra may be too low due to experimental problems. In that case, the yields of projectile fragments must also be significantly higher than deduced above, and whatever renormalisation is necessary for the alpha spectra must also be applied to the deuteron and triton spectra (the proton spectra were measured separately and a different normalisation may conceivably apply). Although incomplete fusion would still account for many of these fragments some might well be attributable to simple break-up processes.

We believe that the observed discrepancy is most likely due to a combination of all three effects. This study has demonstrated conclusively the major contribution of the incomplete-fusion process (^{7}Li,α), and that this is much stronger than the (^{7}Li,t) or (^{7}Li,d) processes, but the conclusions concerning the extent of pure projectile break-up (which can only be inferred indirectly from these measurements) are less precise.

One of the authors (RIB) would like to thank the Hashemite University for financial support of part of this research work. Also two of the authors (RIB) and (IMN) like to thank the research staff at Harwell for their kind hospitality and help during their visit.

References

1. D.J. Parker, J. Asher, T.W. Conlon, I. Naqib, Phys. Rev. C **30**, 143 (1984).
2. D.J. Parker, J.J. Hogan, J. Asher, Phys. Rev. C **39**, 2256 (1989)
3. U. Reus, W. Westmeier, I. Warnecke, At. Data Nucl. Data Tables **29**, 1 (1983).
4. U. Littmark, J.F. Ziegler, *The Stopping and Ranges of Ions in Matter* (Pergamon, New York, 1977) Vol. **6**.
5. F. Pühlhofer, Nucl. Phys. A **280**, 267 (1977).
6. J. Wilczynski, K. Siwek-Wilczynska, Phys. Lett. B **55**, 270 (1975).
7. K. Siwek-Wilczynska, E.H. du Marchie Van Voorthuysen, J. Van Popta, R. H. Siemssen, J. Wilczynski, Nucl. Phys. A **330**, 150 (1979).
8. M. Kicinska-Habior, K.A. Snover, C.A. Gosset, J.A. Behr, G. Feldman, H.K. Glatzel, J H. Gundlach, E.F. Garman, Phys. Rev. C **36**, 612 (1987).
9. M.C. Mermaz, Phys. Rev. C **21**, 2356 (1980).
10. M.C. Mermaz, F. Auger, B. Fernandez, Phys. Rev. C **28**, 1587 (1983); M.C. Mermaz, J. Barrette, H.E. Wegner, Phys. Rev. C **24**, 2148 (1981).
11. M.C. Mermaz, F. Rami, J.P. Coffin, G. Guillaume, B. Heusch, P. Wagner, A. Fahli, P. Fintz, Phys. Rev. C **31**, 1972 (1985).
12. R.I. Badran, I.M. Naqib, D.J. Parker, J. Asher, J. Phys. G: Nucl. Part. Phys. **22**, 1441 (1996).
13. F.J. W. Hahne, Nucl. Phys. A **104**, 545 (1967).
14. J.A. McIntyre, K.H. Wang, L.C. Becker, Phys. Rev. **117**, 1337 (1960); J.A. McIntyre, S.D. Baker, K.H. Wang, Phys. Rev. **125**, 584 (1962).
15. W.E. Frahn, R.H. Venter, Ann. Phys. **24**, 243 (1963).